













[View Journal Online](#)
[View Article Online](#)

Influence of Mg(II) substitution on the structural, magnetic, and permeability properties of R-type hexagonal ferrites

Zahoor Ul Hassan ¹, Imran Sadiq ¹, Hasan Mehmood Khan ², Sajjad Hussain ^{1,*},
 Farhan Sadiq ³, Mishal Idrees ¹, Muhammad Shahbaz ¹, Samreen Saeed ¹,
 Muhammad Imran ⁴, Saira Riaz ¹ and Shahzad Naseem ¹

¹ Centre of Excellence in Solid State Physics, University of the Punjab, Lahore, 54590, Pakistan

² Institute of Physics, The Islamia University of Bahawalpur, Bahawalpur, 63100, Pakistan

³ State Key Laboratory of Fine Chemicals, School of Chemical Engineering, Dalian University of Technology, Dalian 116024, R. P. China

⁴ Department of Physics, Division of Science and Technology, University of Education, Lahore, 54770, Pakistan

* Corresponding author at: Centre of Excellence in Solid State Physics, University of the Punjab, Lahore, 54590, Pakistan.

e-mail: sajjad.phd.cssp@pu.edu.pk (S. Hussain).

RESEARCH ARTICLE



doi: 10.5155/eurjchem.14.2.165-171.2359

Received: 18 November 2022

Received in revised form: 25 January 2023

Accepted: 04 February 2023

Published online: 30 June 2023

Printed: 30 June 2023

KEYWORDS

Sol-gel method
 SEM micrographs
 Magnetic properties
 Structural properties
 Magnetic permeability
 R-Type hexagonal ferrites

ABSTRACT

A series of single-phase R-type hexagonal ferrites with the composition $Sr_{1-x}Mg_xFe_4Sn_2O_{11}$ ($x = 0.0, 0.1, 0.2, 0.3$) were manufactured using the auto-combustion sol-gel method sintered at 800 °C. The objective of this work was to study the effect of Mg additives on the structural, magnetic, and permeability properties of the synthesised material. The X-ray diffraction patterns revealed that all prepared samples have hexagonal structures. The scanning electron micrographs revealed the platelet-like structure of the grains, which would help enhance the magnetic permeability of the materials. Magnetic parameters were investigated in the range of applied field ± 12.5 kOe. The hysteresis loops revealed the paramagnetic nature of all the synthesised samples. With the substitution of Mg contents, the maximum magnetization increased from 1.05 to 2.62 (emu/g) and the remanence from 0.02-0.09 (emu/g), while the coercivity also increased. The magnetic permeability was determined over the frequency range of 20 Hz to 20 MHz. The magnetic permeability of the synthesized hexagonal ferrites is enhanced due to the presence of grains having a platelet-like structure. Furthermore, the particle size calculated using Langevin equations varied in the range of 4.7 to 6.5 nm. The calculated magnetic permeability properties make this synthesised ferrite material useful for super-high-frequency devices.

Cite this: *Eur. J. Chem.* 2023, 14(2), 165-171

Journal website: www.eurjchem.com

1. Introduction

Hexagonal ferrites have enormous applications due to their excellent properties and are especially used as soft/hard magnets [1], magneto-optical devices [2], humidity sensors [3], magnetic recording media [4], microwave absorbers [5], and are also essential systems for military platforms such as radar absorbing materials (RAM) and wireless telecommunication technology such as computer local area networks (LAN) and mobile telephones [6].

R-type hexagonal ferrites ($BaM_2Fe_4O_{11}$) are the notable metal oxides that have recently gained more attention among the hexagonal ferrites group. Generally, R-type hexagonal ferrites possess excellent magnetic and attractive saturation magnetisation, high permeability, high Curie temperature, and excellent chemical stability [7]. The crystal structure of R-type hexagonal ferrite is typically divided into two blocks, R and R*, based on the crystalline structure, where * represents the c-axis with a phase shift of 180° degree. This R-type hexagonal ferrite crystal structure is frustrated by the replacement of oxygen

ions with heavy Ba^{2+}/Sr^{2+} ions and the alteration of accelerated tetragonal sites into bipyramidal trigonal sites. Hence, this leads to magnetic frustration within the magnetic material [8]. It is well established that the substitution of divalent ions within the pure sample alters the structural, magnetic, and magnetic permeability properties of the material [9]. Furthermore, other reasons like the method of synthesis, temperature, and particle size are also key factors for this alteration in magnetic properties [10]. To synthesize all ferrite materials, the sol-gel auto-combustion method is well suited because it requires low-cost materials such as precursor salt [11,12].

This study was aimed at developing soft ferrite based on $Sr_{1-x}Mg_xFe_4Sn_2O_{11}$ ($x = 0.0, 0.1, 0.2, 0.3$), which exhibited a low value of coercivity. Powder X-ray diffraction (XRD) has been done to examine the structural properties of all samples. The scanning electron microscope (SEM) was used to find the grain morphology. The permeability properties have been found for all synthesised materials. Hence, the results predict the possibility that the ferrites could be engineered into desired

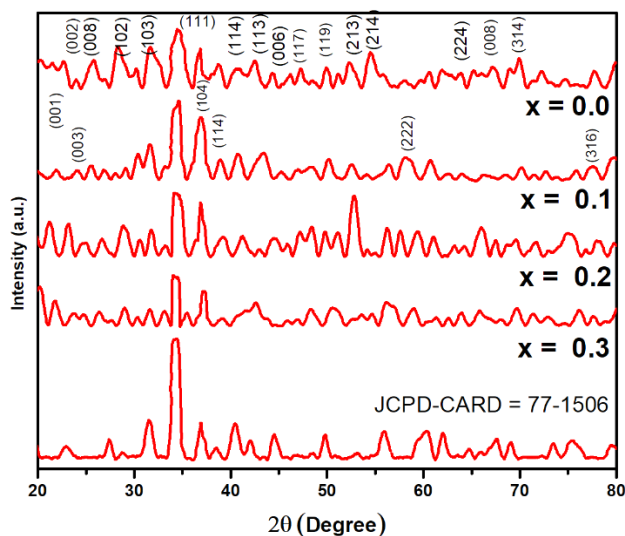
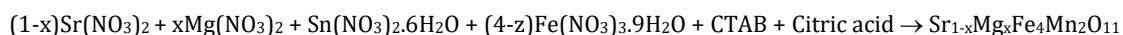


Figure 1. XRD patterns of $\text{Sr}_{1-x}\text{Mg}_x\text{Fe}_4\text{Sn}_2\text{O}_{11}$ with all concentrations ($x = 0.0, 0.1, 0.2,$ and 0.3) of R-type hexagonal ferrites [14].



Scheme 1. Synthesis of $\text{Sr}_{1-x}\text{Mg}_x\text{Fe}_4\text{Sn}_2\text{O}_{11}$.

applications with a precise magnetic response by a suitable choice of microstructure limitations.

2. Experimental

Polycrystalline material, Mg-substituted R-type hexagonal ferrite corresponding to the chemical equation $\text{Sr}_{1-x}\text{Mg}_x\text{Fe}_4\text{Sn}_2\text{O}_{11}$ with various contents ($x = 0.0, 0.1, 0.2, 0.3$) was synthesized by using Sol-gel auto-combustion technique. First, the stoichiometric ratios of CTAB, citric acid ($\geq 99.5\%$), $\text{Sr}(\text{NO}_3)_2$ ($\geq 99.5\%$), $\text{Sn}(\text{NO}_3)_2 \cdot 6\text{H}_2\text{O}$ ($\geq 99.5\%$), $\text{Fe}(\text{NO}_3)_3 \cdot 9\text{H}_2\text{O}$ ($\geq 99.5\%$), and $\text{Mg}(\text{NO}_3)_2 \cdot 6\text{H}_2\text{O}$ ($\geq 99.5\%$) (Sigma-Aldrich) were added in ultrapure deionized water to prepare the aqueous solution. The chemical equation of the reactants and products is Scheme 1.

These solution beakers were then placed on a hot plate to intended for stirring and heating. Continuous stirring is used for 4 hours in the temperature range of 80°C to make the solution homogeneous. During the stirring process, the KOH solution was mixed drop by drop to maintain the pH level of the solution in the range of 7-8 scale [4]. After heating at 80°C and continuously stirring for four hours, a viscous gel of brown colour was obtained. After two hours, the gel was completely burnt and turned into ash. To achieve the fine powder, the ash was ground using an agar mortar pestle for 25 to 30 minutes. This powder was then again heated in a furnace box at a temperature of 800°C for three hours. After this procedure was completed, the resulting samples were ground to obtain the fine powder. Then this ground powder was converted to pellets through a hydraulic press applying the force of 40 KN for 60 seconds. Finally, these pellets were used for the characterization of magnetic properties, XRD, and permeability properties. For structural analysis, the apparatus used for XRD, named Bruker D8 advanced diffractometer (Billerica, Massachusetts) USA, consisted of X-ray radiations of $\text{CuK}\alpha$ source with a wavelength limit of $\lambda = 1.54 \text{ \AA}$. The morphological properties of R-type hexagonal ferrites were analysed by scanning electron microscope (Tokyo, Japan). The developed VSM of Lakshore-740 (Hamburg, New York) USA, records the magnetic hysteresis loops for synthesised R-type hexagonal ferrite under an applied magnetic field up to 12.5 kOe at room temperature (300 K). To investigate the magnetic permeability

properties of the sample at room temperature in the frequency range of 20 Hz to 20 MHz, the impedance analyser model Agilent #E8361A was used.

3. Results and discussion

3.1. Structural characterization

The powder X-ray diffractometer with $\text{Cu-K}\alpha$ radiation source of wavelength ($\lambda = 1.54 \text{ \AA}$) with a scanning rate of $0.8^\circ/\text{min}$ was used to investigate the crystalline phase, the crystalline size, and the lattice parameters of the prepared samples. The XRD patterns of R-type hexagonal ferrites $\text{Sr}_{1-x}\text{Mg}_x\text{Fe}_4\text{Sn}_2\text{O}_{11}$ with concentrations ($x = 0.0, 0.1, 0.2, 0.3$) are depicted in Figure 1. XRD patterns, the unit cell structure, and all other structural parameters of the same materials have already been published in our earlier research paper [13]. The lattice parameter was indexed according to hexagonal ferrite, and, moreover, the crystalline size was in the range of 4.16 to 8.25 nm [13].

3.2. Grain morphology

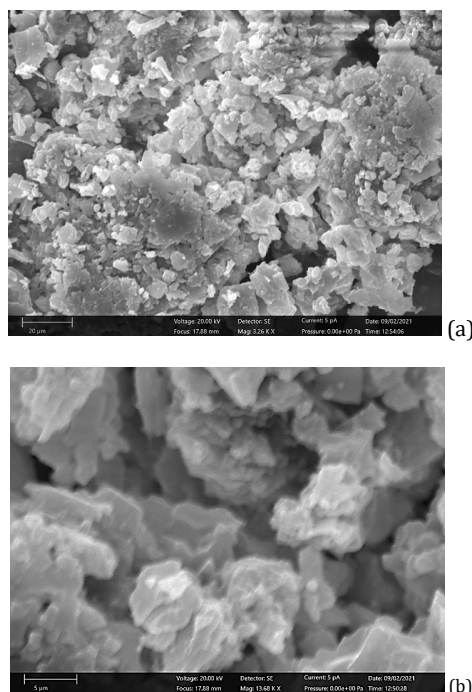
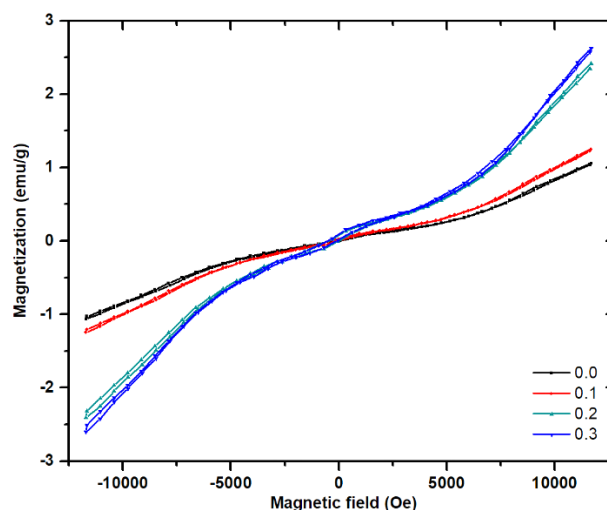
Figure 2 shows low- and high-magnification SEM micrographs of sample R-type hexaferrite $\text{Sr}_{0.7}\text{Mg}_{0.3}\text{Fe}_4\text{Sn}_2\text{O}_{11}$. It can be seen that small particles agglomerate with one another to form large grains. Both micrographs clearly show the platelet structure grains. The small grain size was determined using a line intercept and a range of 28 nm. It is well known that these platelet-like structure grains arrange themselves in response to an externally applied magnetic field, increasing the overall magnetic permeability of the material [14]. As a result, the current synthesised samples can be used in applications requiring high magnetic permeability.

3.3. Magnetic properties

The magnetic nature of the synthesised ferrite materials can be examined by knowing about their magnetic parameters, like maximum magnetization, coercivity (H_c), and remanence (M_r).

Table 1. The values of coercivity (H_c), maximum magnetization, remanence magnetization (M_r), and particle size of $Sr_{1-x}Mg_xFe_4Sn_2O_{11}$ ($x = 0.1, 0.2, 0.3$) R-type hexagonal ferrite.

Mg concentration	Coercivity (Oe)	Maximum magnetization (emu/g)	Remanence magnetization (emu/g)	Particle size (nm)
$x = 0.0$	128	1.05	0.02	6.5
$x = 0.1$	200.5	1.24	0.03	5.7
$x = 0.2$	232.5	2.41	0.07	5.5
$x = 0.3$	223.5	2.62	0.09	4.7

**Figure 2.** Low magnification (a) and high magnification (b) scanning electron micrographs (SEM) of sample $Sr_{0.7}Mg_{0.3}Fe_4Sn_2O_{11}$.**Figure 3.** Magnetic hysteresis loops of $Sr_{1-x}Mg_xFe_4Sn_2O_{11}$ ($x = 0.0, 0.1, 0.2, 0.3$) R-type hexagonal ferrites.

These magnetic parameters can be evaluated from hysteresis loops for different synthesised materials. Figure 3 represents the magnetic hysteresis loops taken under the applied field strength of ± 12.5 kOe for the R-type hexagonal ferrite of composition $Sr_{1-x}Mg_xFe_4Sn_2O_{11}$ ($x = 0.0, 0.1, 0.2, 0.3$) obtained at room temperature (300 K). It was astonishing to observe that all samples exhibited a paramagnetic nature.

The hysteresis parameters of maximum magnetization, remnant magnetization, and coercivity (H_c) are listed in Table 1. It has been observed from hysteresis loops that the values of maximum magnetization and remanence increased with each

substitution of Mg^{2+} ions in pure ferrite. From Table 1, it was observed that for concentration $x = 0.0$, the material has a minimum magnetization value of 1.05 emu/g and a remanence of 0.02 emu/g, which then increases with the substitution of Mg^{2+} ions and it reaches its maximum value of 2.62 emu/g and remanence (0.09 emu/g) for concentration at $x = 0.3$. The following reasons are attributed to this improvement in maximum and remnant magnetization. Tatarchuk *et al.* reported that this increment may be due to the enhancement in the formula unit magnetic moment [15].

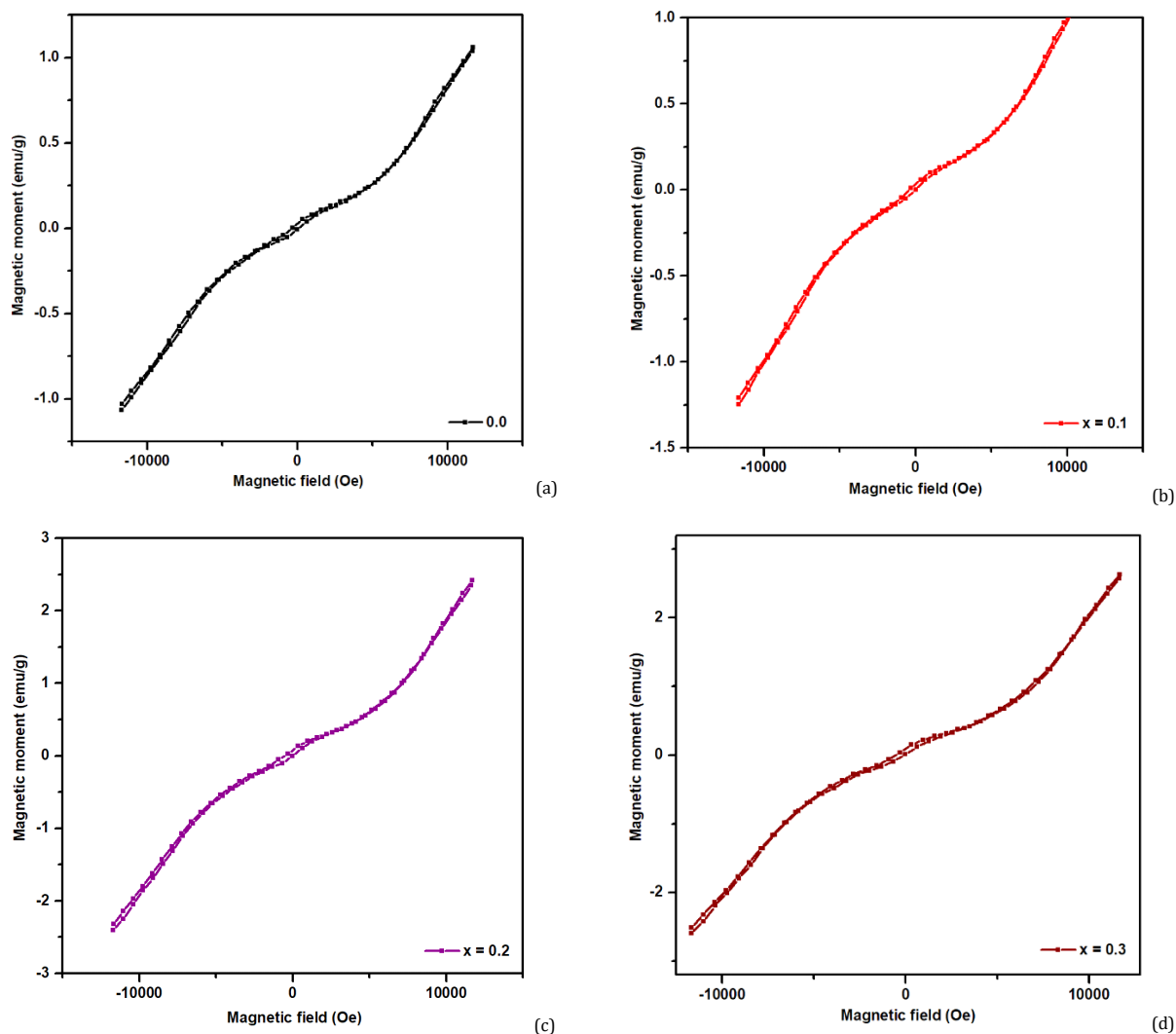


Figure 4. Magnetic hysteresis loops of $\text{Sr}_{1-x}\text{Mg}_x\text{Fe}_4\text{Sn}_2\text{O}_{11}$ R-type hexagonal ferrite ($x = 0.0$ (a), 0.1 (b), 0.2 (c), 0.3 (d)).

Since Mg^{2+} ions possess only two electrons in their outermost electronic configuration of 3s, these both electrons are oriented in the paired up state hence exhibiting magnetic nature. This leads to an increment in the net magnetic moment which is the key point for the enhancement in the overall values of remanence and maximum magnetization. The substitution of Fe^{3+} ions (having spin-up direction) with Mg^{2+} ions increases the magnetization of the material. Narang *et al.* reported that the substitution of Fe^{3+} ions with down-spin (4fI and 4fII) results in the enhancement of magnetization, while the substitution of spin-up Fe^{3+} (12k, 2a, 2b) causes a decrease in net magnetization [16]. Table 1 shows the worth-noting point that the value of coercivity for the pure sample is minimum 128 Oe, which then enhances with Mg doping and reaches to its maximum value of 233.5 Oe for a doping concentration of additives $x = 0.2$.

The Langevin function was also used to determine particle sizes [17]:

$$M(H) = M_s L(y) \quad (1)$$

and

$$L(y) = \text{Coth}(y) - \frac{1}{y} \quad (2)$$

$$y = \mu_0 \mu H(y) - \frac{1}{y} \quad (3)$$

Here (μ_0) vacuum permeability, (μ) magnetic moments of nanoparticles, (H) applied magnetic field, (K_B) Boltzmann constant and (T) Temperature. For a given temperature, the particle sizes are estimated using formula [18];

$$D^3 = \frac{18 K_B T \chi}{\pi \mu_0 M_s^2} \quad (4)$$

The estimated particle size values of the substituted samples with rare earth elements are calculated using expression (4). From the M-H loop, the volume susceptibility χ of the samples is also calculated. The saturation magnetisation values of the nanoparticles are determined by working with the expressions (1) and (2). The particle sizes values for each sample, calculated using the above formulations, are given in Table 1. The coercivity of the material is directly related to particle size; with Mg substitution, the size of the sample particles decreases throughout the Mg doping, so the value of coercivity increased and reaches its maximum value at Mg concentration of $x = 0.2$ [18]. So, at that time, the multi-domain material becomes converted into a single domain below the critical point, then the material exhibits the paramagnetic nature, hence the hysteresis loop becomes shortened as depicted in Figure 4 for all substitutions.

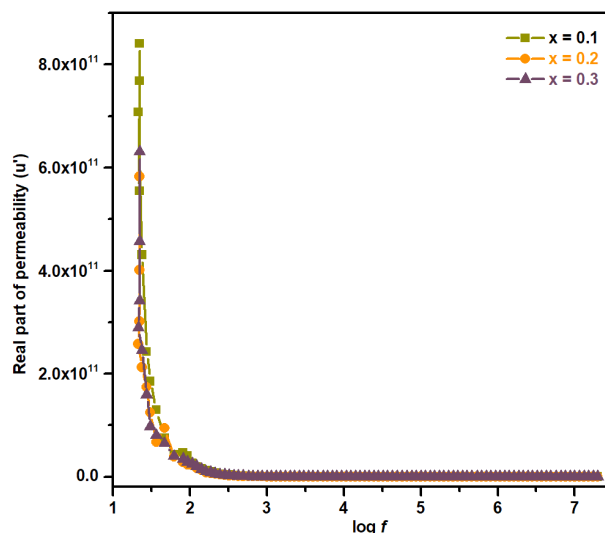


Figure 5. Variation of the real part μ' of complex permeability versus frequency for $\text{Sr}_{1-x}\text{Mg}_x\text{Fe}_4\text{Sn}_2\text{O}_{11}$ ($x = 0.1, 0.2, 0.3$) R-type hexagonal ferrites.

Another remarkable reason is that, in hexagonal ferrites, the c -axis also plays an active role in reducing coercivity. When the magnetic field is applied in a perpendicular manner, the loosely orientated crystals try to orient themselves along the c -axis. Therefore, the substitution of Mg^{2+} ions that possess large ionic radii leads to the production of more disruption in the crystal lattice that might enhance the magnetic crystalline anisotropy, thus increasing the value of coercivity [19]. It was worth noted that the magnetic parameters determine from magnetic loops. From the M_s values suggested that this $\text{Sr}_{1-x}\text{Mg}_x\text{Fe}_4\text{Sn}_2\text{O}_{11}$ ($x = 0.0, 0.1, 0.2, 0.3$) R-type hexagonal ferrite possesses paramagnetic nature.

3.4. Magnetic permeability analysis

The permeability behavior is one of the most imperative characteristics of ferrites, which significantly influenced by the preparation situations, *e.g.*, sintering time, additive amount, type, and temperature. The magnetic permeability properties of all samples were measured at 300 K over the 20-Hz to 20-MHz frequency range. The variation of the real part of the permeability with frequency is illustrated in Figure 5. The trend clearly demonstrated that the real (μ') part of permeability exhibited high values at low frequency and dropped rapidly and became constant with the increase of frequency. Several factors are responsible for the change in permeability properties of the material like crystallinity, process of magnetization (spin rotation occurring in single domain grain, movement of domain-wall occurring in multi-domain grain) and grain volume [20]. Generally, at higher frequencies, the domain wall is damped and does not respond during applied electric and magnetic field oscillations and only spin rotation occurs at higher frequency ranges. The worthwhile relation between initial permeability and resonant frequency f_R is given by a law known as Snoek's law [21].

$$f_R = \frac{1}{\mu_i} \times 3 \times 10^9 \text{ Hz} \quad (5)$$

Snoek's law represents the reciprocal relationship between resonance frequency and initial permeability (μ_i). Therefore, the permeability decreases rapidly in all substituted samples at a lower frequency while it becomes constant extremely near zero, consequently with further increment in frequency. The decrease in real permeability may be due to the porosity that arose during the sintering process of the ferrite samples. This

porosity may hinder the domain-wall motion during magnetization, which leads to a decrease in the real part of the permeability. Moreover, this rapid reduction in permeability at higher frequencies might be due to the vibrational frequency that does not match the domains of the material with the applied magnetic field [22].

The decreasing behaviour of the imaginary part (μ'') of the complex permeability as a function of frequency can be observed in Figure 6. This behaviour of μ'' can be explained on the basis of Snoek's law. According to the Snoek model, the relationship between μ'' and frequency (resonance frequency) is expressed as;

$$f_{\text{res}} = \frac{\gamma M_s}{4\pi\mu''\alpha} \quad (6)$$

where α is the extinction coefficient, while M_s represents the saturation magnetisation. This model indicates the inverse relation between μ'' (loss factor) and f_{res} .

Various remarkable factors are involved in altering the (μ'') as well as the resonance frequency. Figure 5 demonstrated that Mg additives altered the maximum value of permeability for each sample, which also changed the characteristic frequencies as a consequence of both the respective relaxation of the domain wall and the ferromagnetic resonance. This relaxation process may cause to generate microwave dissipation, which leads to the creation of thermal energy.

As a consequence, the value of μ'' starts to decrease rapidly with increasing frequency [22]. Moreover, the Mg doping leads in a decrease in magneto-crystalline anisotropy, which may lead to a drop in domain-wall hardness and a subsequent fall in resonance frequency. As a consequence, the contribution of these two mechanisms tends to increase the permeability levels with the Mg content. So, it may conclude that at lower frequency regions the μ'' is reciprocal to magneto-crystalline anisotropy [23].

The complex imaginary part of the permeability (μ'') reveals the observed magnetic loss. The varying trend of tan loss with frequency can be clearly seen for all Mg-substituted samples with concentrations $x = 0.1, 0.2, \text{ and } 0.3$ taken at 300 K, as shown in Figure 7. This may be due to the exchanging electron mechanism between Fe^{3+} and Fe^{2+} ions in the lower frequency zone, which requires more energy, representing high magnetic loss in the low frequency range.

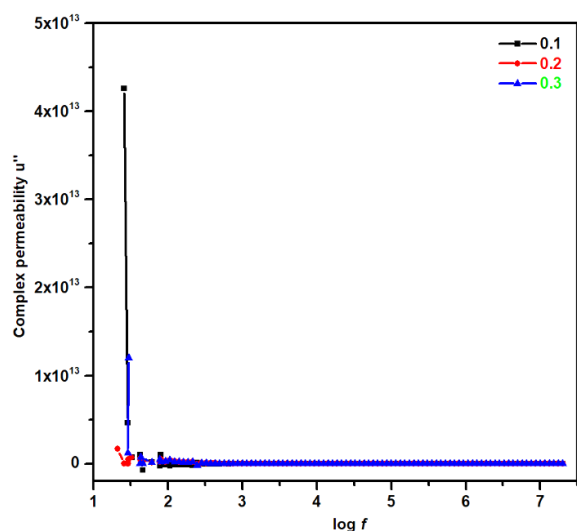


Figure 6. Variation of the imaginary part μ'' of the complex permeability versus frequency for $\text{Sr}_{1-x}\text{Mg}_x\text{Fe}_4\text{Sn}_2\text{O}_{11}$ ($x = 0.1, 0.2, 0.3$) R-type hexagonal ferrites.

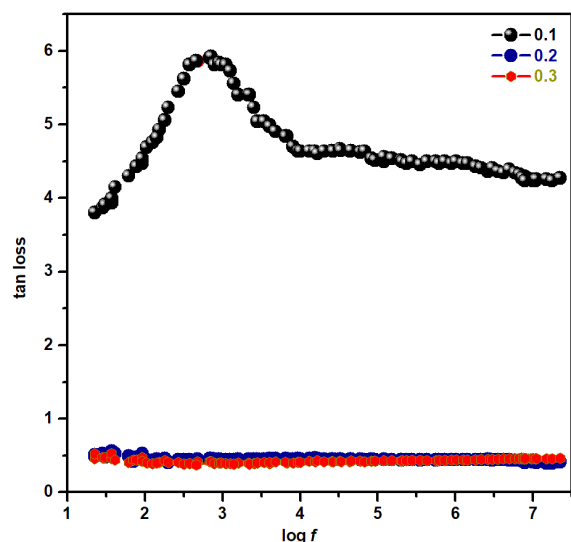


Figure 7. Graph of tan loss (magnetic loss) versus frequency of Mg-doped $\text{Sr}_{1-x}\text{Mg}_x\text{Fe}_4\text{Sn}_2\text{O}_{11}$ R-type hexagonal ferrite at the concentration ($x = 0.1, 0.2, 0.3$).

The frequency spectrum represents the observed resonant peak for $x = 0.1$ at about 2.83 MHz. These attributed peaks arose due to the matching behaviour of two frequencies, one the frequency of the applied field, while the other is the frequency between Fe^{3+} and Fe^{2+} ions, known as the hopping frequency. When both these frequencies, the hopping frequency of the electron and the frequency of the applied field, match each other, a phenomenon, known as resonance phenomena, occurs, which is responsible for generating these resonant peaks in higher-frequency regions. This is why these peaks are known as resonant peaks, as they come from frequency resonance phenomena [24].

Due to experimental restrictions, resonant peaks could not be demonstrated for the synthesized material at $x = 0.2$ and 0.3 which may also exist at higher range of frequencies. Generally, magnetic losses are required to examine the ferrite material's magnetic permeability properties. The crystal defects as well as the impurities are responsible for the high resistance. At high frequencies, low-resistive grains become much more active, causing the dielectric constant to decrease [25]. The findings indicate that magnetic loss has increased, demonstrating

greater alteration of the magnetic permeability features of ferrites [26].

4. Conclusions

The autocombustion sol-gel procedure was used to synthesise the divalent element 'Mg successfully' substituted R-type hexagonal ferrites $\text{Sr}_{1-x}\text{Mg}_x\text{Fe}_4\text{Sn}_2\text{O}_{11}$ ($x = 0.0, 0.1, 0.2, 0.3$). For all samples, the XRD graphs revealed a single R-type hexagonal ferrite phase. Because of the substitution of the Fe^{3+} ions, which perturbed the exchange interaction strength in the material, the maximum value of magnetization and remanence magnetization increased. The substitution of Mg content increased the coercivity of all samples. The particle size was calculated using the Langevin function and ranged from 4.7 to 6.5 nm. The M-H loops demonstrated that the synthesised samples were paramagnetic in nature. These ferrite materials are useful for super high-frequency devices due to their increased magnetic permeability (SHF).

Acknowledgements

Special thanks from the author to Director, Centre of Excellence in Solid State Physics, University of Punjab, Lahore, for providing all research facilities.

Disclosure statement


Conflict of interests: The authors declare that they have no conflict of interest. Ethical approval: All ethical guidelines have been adhered. Sample availability: Samples of the compounds are available from the author.

CRedit authorship contribution statement

Conceptualization: Zahoor Ul Hassan, Imran Sadiq; Methodology: Mishal Idrees; Software: Saira Riaz; Validation: Hassan mehmoood Khan; Formal Analysis: Muhammad Sahahbaz Qureshi; Investigation: Samreen Saeed; Resources: Shahzad Naseem; Data Curation: Farhan Sadiq; Writing - Original Draft: Sajjad Hussain; Zahoor Ul Hassan, Imran Sadiq; Writing - Review and Editing: Sajjad Hussain; Muhammad Imran Visualization: Imran Sadiq; Funding acquisition: Saira Riaz; Supervision: Imran Sadiq Khan; Project Administration: Imran Sadiq.

ORCID and Email

Zahoor Ul Hassan

 zahoor507499@gmail.com


 <https://orcid.org/0000-0003-0372-9502>


Imran Sadiq

 imran.cssp@pu.edu.pk

 <https://orcid.org/0000-0002-6583-8168>

Hasan Mehmood Khan

 hmkhan@iub.edu.pk

 <https://orcid.org/0000-0002-9440-5580>

Sajjad Hussain

 sajjad.phd.cssp@pu.edu.pk

 <https://orcid.org/0000-0001-6145-0484>

Farhan Sadiq

 farhansadiq.khan@yahoo.com


 <https://orcid.org/0000-0001-5487-3622>


Mishal Idrees

 mishal.phd.cssp@pu.edu.pk

 <https://orcid.org/0000-0001-8292-8926>


Muhammad Shahbaz

 msq351@gmail.com

 <https://orcid.org/0000-0002-8738-2851>


Samreen Saeed

 samreensaheed489@gmail.com

 <https://orcid.org/0000-0001-6871-7639>

Muhammad Imran

 m.imran@ue.edu.pk

 <https://orcid.org/0000-0003-1128-147X>

Saira Riaz

✉ saira.cssp@pu.edu.pkORCID <https://orcid.org/0000-0003-4720-1996>

Shahzad Naseem

✉ shahzad.cssp@pu.edu.pkORCID <https://orcid.org/0000-0002-7814-7577>

References

- [1]. Hiratsuka, N. Soft magnetic hexagonal ferrites for high frequency devices. *J. Magn. Soc. Jpn.* **2013**, *37*, 141–146.
- [2]. Yousaf, M.; Nazir, S.; Hayat, Q.; Akhtar, M. N.; Akbar, M.; Lu, Y.; Noor, A.; Zhang, J.-M.; Shah, M. A. K. Y.; Wang, B. Magneto-optical properties and physical characteristics of M-type hexagonal ferrite (Ba_{1-x}CaxFe_{11.4}Al_{0.60}19) nanoparticles (NPs). *Ceram. Int.* **2021**, *47*, 11668–11676.
- [3]. Vaingankar, A. S.; Kulkarni, S. G.; Sagare, M. S. Humidity Sensing using Soft Ferrites. *J. Phys. IV* **1997**, *07*, C1-155-C1-156.
- [4]. Gerber, R.; Atkinson, R.; Šimša, Z. Magnetism and magneto-optics of hexaferrite layers. *J. Magn. Magn. Mater.* **1997**, *175*, 79–89.
- [5]. Singh, J.; Singh, C.; Kaur, D.; Narang, S. B.; Jotania, R. B.; Ateia, E.; Kagdi, A.; Joshi, R.; Sombra, A. S. B.; Zhou, D.; Trukhanov, S.; Panina, L. Development of doped Ba–Sr hexagonal ferrites for microwave absorber applications: Structural characterization, tunable thickness, absorption peaks and electromagnetic parameters. *J. Alloys Compd.* **2021**, *855*, 157242.
- [6]. Kumar, A.; Agarwala, V.; Singh, D. Effect of mg substitution on microwave absorption of BaFe₁₂O₁₉. *Adv. Mat. Res.* **2012**, *585*, 62–66.
- [7]. Amjad, T.; Sadiq, I.; Javaid, A. B.; Riaz, S.; Naseem, S.; Nadeem, M. Investigation of structural, electrical, electrical polarization and dielectric properties of CTAB assisted Ni²⁺ substituted R-type nanohexaferrites. *J. Alloys Compd.* **2019**, *770*, 1112–1118.
- [8]. Kagdi, A. R.; Solanki, N. P.; Carvalho, F. E.; Meena, S. S.; Bhatt, P.; Pullar, R. C.; Jotania, R. B. Influence of Mg substitution on structural, magnetic and dielectric properties of X-type barium zinc hexaferrites Ba₂Zn_{2-x}MgxFe₂₈O₄₆. *J. Alloys Compd.* **2018**, *741*, 377–391.
- [9]. Shahbaz, M.; Sadiq, I.; Butt, M. M. H.; Basit Javaid, A.; Idrees, M.; Hussain, S.; Sadiq, F.; Riaz, S.; Naseem, S.; Khan, H. M. Peculiar magnetic behavior and structural, electrical, dielectric properties of substituted R-type hexagonal ferrites. *J. Magn. Magn. Mater.* **2020**, *499*, 166309.
- [10]. Rana, G.; Johri, U. C.; Asokan, K. Correlation between structural and dielectric properties of Ni-substituted magnetite nanoparticles. *EPL* **2013**, *103*, 17008.
- [11]. Mammo, T. W.; Murali, N.; Kumari, C. V.; Margarette, S. J.; Ramakrishna, A.; Vemuri, R.; Shankar Rao, Y. B.; Vijaya Prasad, K. L.; Ramakrishna, Y.; Samatha, K. Synthesis, structural, dielectric and magnetic properties of cobalt ferrite nanomaterial prepared by sol-gel autocombustion technique. *Physica B Condens. Matter* **2020**, *581*, 411769.
- [12]. Iqbal, M. J.; Ashiq, M. N.; Gomez, P. H. Effect of doping of Zr–Zn binary mixtures on structural, electrical and magnetic properties of Sr-hexaferrite nanoparticles. *J. Alloys Compd.* **2009**, *478*, 736–740.
- [13]. Hussain, S.; Sadiq, I.; Khan, H. M.; Idrees, M.; Sadiq, F.; Shah, A.; Riaz, S.; Naseem, S. Characterization and curve fittings of Mg²⁺ substituted R-type hexagonal ferrites. *Physica B Condens. Matter* **2021**, *605*, 412642.
- [14]. Pullar, R. C. Hexagonal ferrites: A review of the synthesis, properties and applications of hexaferrite ceramics. *Prog. Mater. Sci.* **2012**, *57*, 1191–1334.
- [15]. Tatarchuk, T. R.; Paliychuk, N. D.; Bououdina, M.; Al-Najar, B.; Pacia, M.; Macyk, W.; Shyichuk, A. Effect of cobalt substitution on structural, elastic, magnetic and optical properties of zinc ferrite nanoparticles. *J. Alloys Compd.* **2018**, *731*, 1256–1266.
- [16]. Narang, S. B.; Singh, C.; Bai, Y.; Hudiara, I. S. Microstructure, hysteresis and microwave absorption analysis of Ba(1-x)Sr_xFe₁₂O₁₉ ferrite. *Mater. Chem. Phys.* **2008**, *111*, 225–231.
- [17]. Fonseca, F. C.; Goya, G. F.; Jardim, R. F.; Muccillo, R.; Carreño, N. L. V.; Longo, E.; Leite, E. R. Superparamagnetism and magnetic properties of Ni nanoparticles embedded in SiO₂. *Phys. Rev. B Condens. Matter* **2002**, *66*, 104406.
- [18]. Drofenik, M.; Ban, I.; Makovec, D.; Žnidaršič, A.; Jagličič, Z.; Hanžel, D.; Lisjak, D. The hydrothermal synthesis of super-paramagnetic barium hexaferrite particles. *Mater. Chem. Phys.* **2011**, *127*, 415–419.
- [19]. Shams, M. H.; Salehi, S. M. A.; Ghasemi, A. Electromagnetic wave absorption characteristics of Mg–Ti substituted Ba-hexaferrite. *Mater. Lett.* **2008**, *62*, 1731–1733.
- [20]. Ibrahim, I. R.; Hashim, M.; Nazlan, R.; Ismail, I.; Wan Ab Rahman, W. N.; Abdullah, N. H.; Mohd Idris, F.; Shafie, M. S. E.; Muhamad Zulkimi, M. M. Grouping trends of magnetic permeability components in their parallel evolution with microstructure in Ni_{0.3}Zn_{0.7}Fe₂₀O₄. *J. Magn. Magn. Mater.* **2014**, *355*, 265–275.
- [21]. Goldman, A. *Handbook of modern ferromagnetic materials*; 1999th ed.; Springer: New York, NY, 2012.
- [22]. Widanarto, W.; Effendi, M.; Ghoshal, S. K.; Kurniawan, C.; Handoko, E.; Alaydrus, M. Bio-silica incorporated barium ferrite composites: Evaluation of structure, morphology, magnetic and microwave absorption traits. *Curr. Appl. Phys.* **2020**, *20*, 638–642.
- [23]. Stergiou, C. A.; Litsardakis, G. Y-type hexagonal ferrites for microwave absorber and antenna applications. *J. Magn. Magn. Mater.* **2016**, *405*, 54–61.
- [24]. Soman, V. V.; Nanoti, V. M.; Kulkarni, D. K. Dielectric and magnetic properties of Mg–Ti substituted barium hexaferrite. *Ceram. Int.* **2013**, *39*, 5713–5723.
- [25]. Amin, M.; Rafique, H. M.; Mustafa, G. M.; Mahmood, A.; Ramay, S. M.; Atiq, S.; Ali, S. M. Effect of La/Cr co-doping on dielectric dispersion of phase pure BiFeO₃ nanoparticles for high frequency applications. *J. Mater. Res. Technol.* **2021**, *13*, 1534–1545.
- [26]. Mruczkiewicz, M.; Krawczyk, M.; Mikhaylovskiy, R. V.; Kruglyak, V. V. Towards high-frequency negative permeability using magnonic crystals in metamaterial design. *Phys. Rev. B Condens. Matter Mater. Phys.* **2012**, *86*, 024425.



Copyright © 2023 by Authors. This work is published and licensed by Atlanta Publishing House LLC, Atlanta, GA, USA. The full terms of this license are available at <http://www.eurjchem.com/index.php/eurjchem/pages/view/terms> and incorporate the Creative Commons Attribution-Non Commercial (CC BY NC) (International, v4.0) License (<http://creativecommons.org/licenses/by-nc/4.0>). By accessing the work, you hereby accept the Terms. This is an open access article distributed under the terms and conditions of the CC BY NC License, which permits unrestricted non-commercial use, distribution, and reproduction in any medium, provided the original work is properly cited without any further permission from Atlanta Publishing House LLC (European Journal of Chemistry). No use, distribution, or reproduction is permitted which does not comply with these terms. Permissions for commercial use of this work beyond the scope of the License (<http://www.eurjchem.com/index.php/eurjchem/pages/view/terms>) are administered by Atlanta Publishing House LLC (European Journal of Chemistry).